Supporting Information

Streeter and Dugmore 10.1073/pnas.1220161110

SI Text

Field Data Collection

Field data were collected from six sites in south Iceland (Table S1) affected by tephra fall from the eruptions of Eyjafjallajökull in April 2010 (Ey2010) and Grímsvötn in May 2011 (G2011). Transect sites T1 and T2 were located within the fallout area for Ey2010, where the initial tephra deposition was 40–50 mm at T1 and 30–40 mm at T2 (1). Maps of the G2011 fallout have not yet been published. Field sites T3–T6 were selected to have 30–50 mm of fine-grained G2011 tephra, and thus to be similar to those selected from Ey2010. The locations of transects, slope angles, and geomorphological details are shown in Table S1. All sites were located from 120–145 m above sea level in areas of contemporary outfield grazing. The modern vegetation consists of forb meadow, grassland, and moss banks (2, 3), it and ranges from complete coverage to none. All study sites lie within the presettlement *Betula* woodlands of Iceland (4), and the present open landscape with discontinuous vegetation cover and active soil erosion is a result of 1,200 y of human actions, climate change, and volcanic impacts (5, 6). Photographs show vegetation cover in June 2012 and the key geomorphological features (Fig. S1).

The modification of tephra exposed at the surface is swift and comprehensive because of its lack of cohesion and the wide range of commonly occurring meteorological conditions that can mobilize these sediments (7, 8). The recently deglaciated forelands of Eyjafjallajökull immediately to the south of the 2010 eruption received some of the greatest depths of fallout, yet observations undertaken as part of the research reported here show that within 2 y, these areas had been effectively stripped clean of exposed tephra. Once incorporated within the root mat and surface andisol stratigraphy, morphological change of the tephra layer is dramatically reduced; bioturbation is limited due to the depauperate nature of the Icelandic biota and the prevailing climate. Cryoturbation, where it exists, produces easily recognizable structures (9, 10).

Climate

The climate of Iceland has warmed since the early 1980s, although there is significant interannual variability (11). At Kirkjubæjarklaustur (~25 km southwest from T3–T6), the number of days per year with temperatures below 0 °C has declined over the past 20 y, from 118 ± 13.1 (average ± 1 SD, 1992–2002) to 105 ± 13.7 (average ± 1 SD, 2003–2011). This means that processes related to and intensified by cold temperatures, such as cryoturbation, are also likely to be in decline.

Data Analysis

Both the original thickness measurements and the residuals of detrended datasets were analyzed for the presence of early warning signals. Detrending was achieved using a Gaussian filter to remove long-term trends and high-frequency variation. A rolling, two-sided window of bandwidth $n = 30$ (480 mm of transect length) was used for the filter. This filter size is 5–17% of the dataset, depending on the length of the transect. These filter sizes are comparable to filters used by others (12), and it was confirmed by visual inspection that this methodology did not overfit the data and reduce the short-term variations we were interested in.

Three metric-based indicators of early warning signals were calculated. Increasing autocorrelation indicates rising memory in the system (13); in this study, it was the correlation coefficient of a first-order autoregressive model computed in the R package earlywarnings, version 1.0.2 (12). Increases in SD were used to evaluate increasing variability in the system (14). Change in skewness is an indicator of a system moving between two stability domains (15), and this indicator was calculated for T1 and T6. All metric indicators were calculated for a rolling window half the length of the dataset (Table S1). In addition, the moving average skewness of the last 30 data points was calculated for transect T1.

To determine the strength of observed trends, the nonparametric Kendall τ rank correlation coefficient statistic was calculated for both the original and detrended datasets (two-tailed at $P = 0.05$ significance).

Sensitivity Analysis

Trends in autocorrelation and SD within detrended datasets are sensitive to choices made in both the rolling window size and the filtering bandwidth (12, 13). To assess the sensitivity of our analysis, we calculated the Kendall τ rank correlation coefficient statistic for trends in autocorrelation and SD for a range of rolling window and bandwidth sizes. Window sizes of 25–75% of the dataset length (increasing in increments of five) and filtering bandwidths of 2–50% (in increments of five) were evaluated. The sensitivity of SD and autocorrelation is presented in Fig. S2. Because all transects were collected with the same sampling interval, we followed best practice (12) and used a consistent bandwidth filter size across all transects.

Significance Testing

As well as testing for sensitivity, it is important to assess the probability that the observed indicator trends are due to chance (12). Probability assessment was done in this study using the *surrogates_ews* function in the R package earlywarnings, version 1.0.2. This fits a linear autoregressive moving average model to the data and then generates 1,000 surrogate datasets of the same size as the original. Then, the Kendall τ correlation coefficient is calculated for each surrogate dataset and compared with the Kendall τ value for the real data. The frequency at which the simulated Kendall τ value is equal to or larger than the original is P, the probability that the trend was due to chance (12).

The probability scores for both the original and detrended datasets are shown in Table S2.

1. Gudmundsson MT, et al. (2012) Ash generation and distribution from the April-May 2010 eruption of Eyjafjallajökull, Iceland. *Sci Rep* 2:572.
2. Kristjansson H (1998) *A Guide to the Flowering Plants and Ferns of Iceland* (Mál og Menning, Reykjavík, Iceland), 2nd Ed.
3. Icelandic Institute of Natural History (2012) Major vegetation types in Iceland. Available at http://en.ni.is/botany/vegetation/vegetation-types/. Accessed March 14, 2013.
4. Hallsdóttir M (1987) Pollen analytical studies of human influence on vegetation in relation to the Landnám tephra layer in southwestern Iceland*Lundqua Thesis* 18181–45.
5. Dugmore AJ, Gísladóttir G, Simpson IA, Newton A (2009) Conceptual models of 1200 years of Icelandic soil erosion reconstructed using tephrochronology. *Journal of the North Atlantic* 2:1–18.
6. Crofts R (2011) *Healing the Land* (Gunnarsholt: Soil Conservation Service of Iceland, Gunnarsholt, Iceland).
7. Arnalds O (2000) The Icelandic 'rofabard' soil erosion features. *Earth Surface Processes and Landforms* 25:17–28.
8. Arnalds O, Gisladottir FO, Orradottir B (2012) Determination of aeolian transport rates of volcanic soils in Iceland. *Geomorphology* 167:4–12.
9. Kirkbride MP, Dugmore M (2005) *Cryospheric Systems: Glaciers and Permafrost*, eds Harris C, Murton J (Geological Society, London), pp 145–155.
10. Dugmore AJ, Newton A (2012) Isochrons and beyond: Maximizing the use of tephrochronology in geomorphology. *Jökull* 62:39–52.
11. Hanna E, Jónsson T, Box JE (2004) An analysis of Icelandic climate since the nineteenth century. *Int J Climatol* 24:1193–1210.

12. Dakos V, et al. (2012) Methods for detecting early warnings of critical transitions in time series illustrated using simulated ecological data. *PLoS ONE* 7(7):e41010.
13. Dakos V, et al. (2008) Slowing down as an early warning signal for abrupt climate change. *Proc Natl Acad Sci USA* 105(38):14308–14312.
14. Carpenter SR, Brock WA (2006) Rising variance: A leading indicator of ecological transition. *Ecol Lett* 9(3):311–318.
15. Guttal V, Jayaprakash C (2008) Changing skewness: An early warning signal of regime shifts in ecosystems. *Ecol Lett* 11(5):450–460.

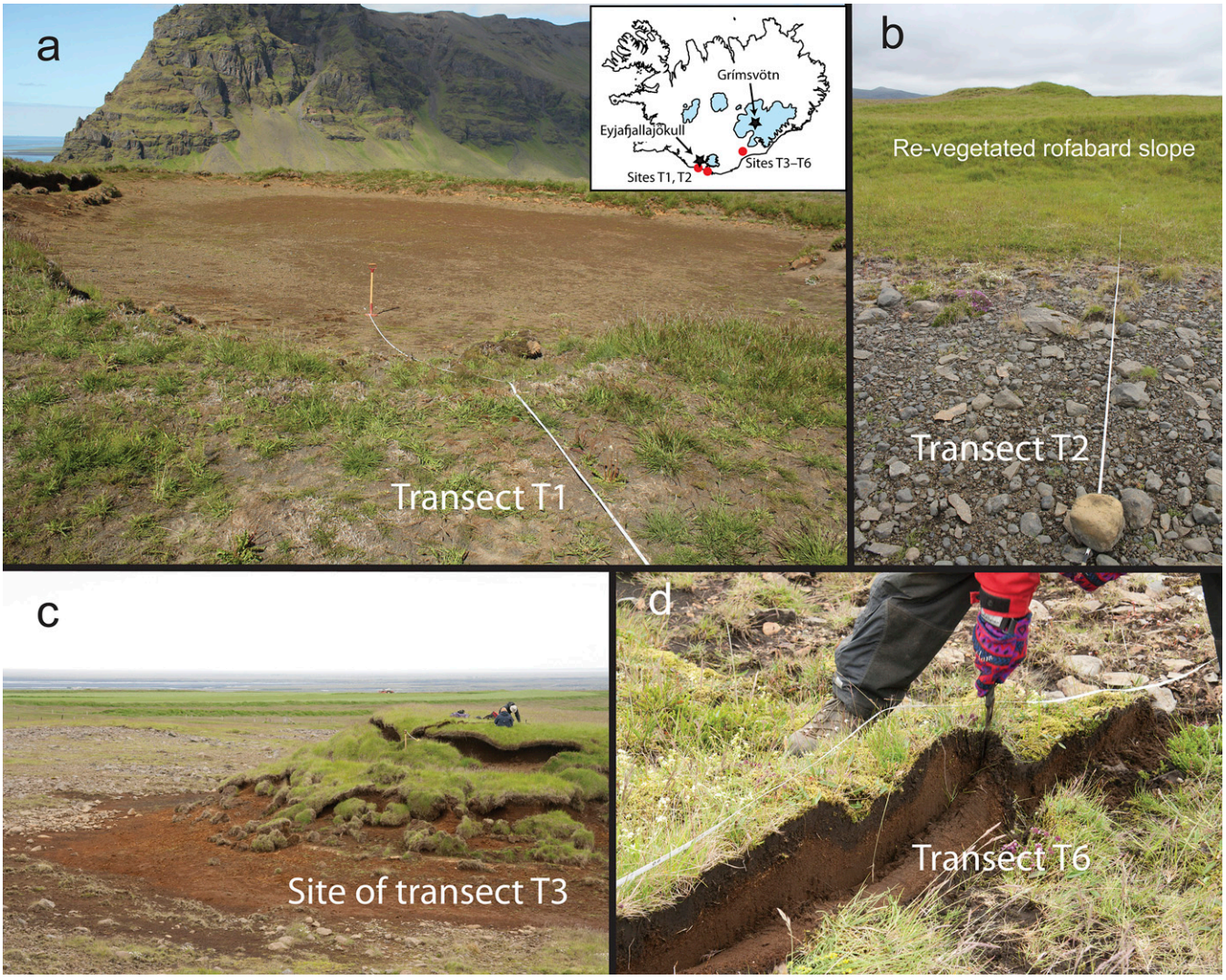

Fig. S1. Photographs of land surface transitions and recent tephra layers within the vegetation and map of source volcanoes for tephra and study sites. Inset in *A* shows the location of the transects (T1–T6) and volcanoes Eyjafjallajökull and Grímsvötn. (*A*) Location of T1 (shown by the tape measure) as it spans the edge of a deflation hollow. (*B*) Location of T2 (shown by the tape measure) with a revegetated rofabard slope in the background. (*C*) Rofabard erosion shows the exposed substrate, eroding andisol slope, and vegetated surface. T3 runs from the figures to top of the eroding slope. (*D*) Tephra from G2011 in T6 has experienced rapid stabilization within surface vegetation (photographed in June 2012). The tephra (uppermost gray-black layer) is clearly distinguished from the brown andisol. The form of the tephra layer mirrors the preexisting land surface.

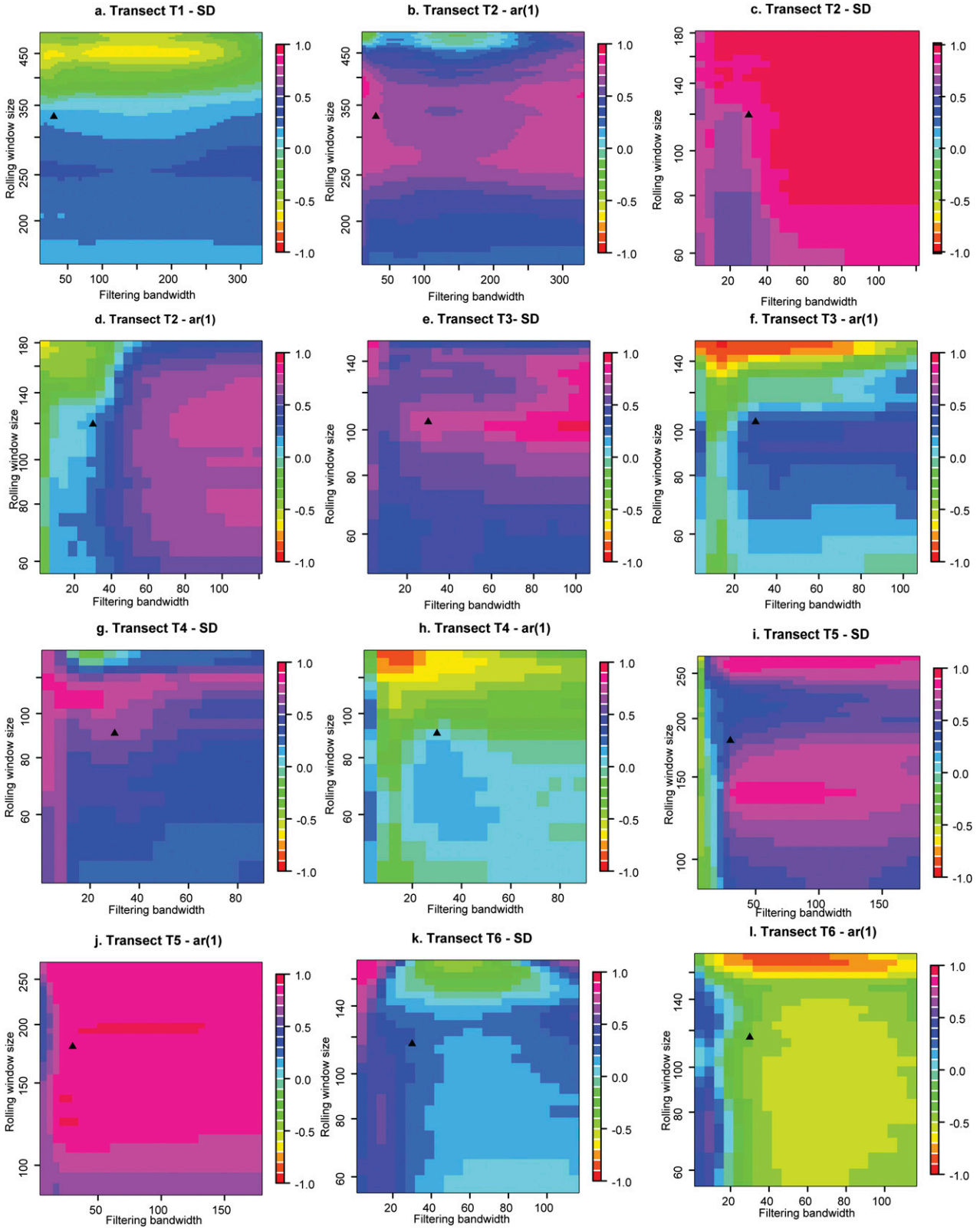

Fig. S2. Sensitivity of trends in autocorrelation and SD as measured by the Kendall τ rank correlation coefficient to choices in rolling window size and filtering bandwidth. The black triangle indicates the size of the rolling window and filtering bandwidth used in analysis. ar(1), autoregressive model of order 1.

Table S1. Details of transects, including location, length, type of land surface transition, and rolling window size used

Transect	Land surface start	Land surface end	Longitude	Latitude	Altitude, m asl	Slope angle, °	*N*	Total transect length, m	Rolling window size
T1	Vegetated andisol (grasses/forbs/moss)	Deflating andisol	W 19° 38′ 370″	N 63° 32′ 874″	200	3	663	10.61	332
T2	Vegetated andisol (grasses/forbs/moss)	Exposed diamicton	W 19° 22′ 370″	N 63° 30′ 466″	150	2	239	3.82	120
T3	Vegetated andisol (grasses/forbs/moss)	Edge of eroding andisol (rofabard)	W 17° 39′ 546″	N 63° 57′ 552″	120	3	208	3.33	104
T4	Vegetated andisol (grasses/forbs/moss)	Edge of eroding andisol (rofabard)	W 17° 39′ 781″	N 63° 57′ 874″	130	3	181	2.90	91
T5	Vegetated andisol (grasses/forbs/moss)	Earth hummock (thufur)	W 17° 39′ 671″	N 63° 57′ 737″	130	7	359	5.74	180
T6	Vegetated andisol (grasses/forbs/moss)	Cryoturbation of surface clasts	W 17° 39′ 350″	N 63° 57′ 628″	145	8	232	3.71	116

asl, above sea level.

Table S2. Probability values that the observed Kendall τ trend values were due to chance

	Original data			Residuals of detrended data		
Transect	SD	ar(1)	Skewness	SD	ar(1)	Skewness
T1	0.138	0.001	0.111	0.153	0.001	0.114
T2	0.014	0.01		0.013	0.018	
T3	0.001	0.121		0.001	0.126	
T4	0.053	0.143		0.058	0.147	
T5	0.109	0.001		0.11	0.006	
T6	0.002	0.257	0.619	0.003	0.264	0.948
Combined probability*	$<1^{-5}$	$<1^{-5}$		$<1^{-5}$	$<1^{-4}$	

Probability values were calculated by summing the frequency that the Kendall τ trend values larger than the original Kendall τ trend value were found in a set of 1,000 surrogate datasets.
*Calculated using Fisher's combined probability method.